A Chandra X#Ray Study of the Globular Cluster M80

The Astrophysical Journal, 598:516–526, 2003 November 20

A *CHANDRA* X-RAY STUDY OF THE GLOBULAR CLUSTER M80

C. O. Heinke, J. E. Grindlay, P. D. Edmonds, D. A. Lloyd, and S. S. Murray
Harvard College Observatory, 60 Garden Street, Cambridge, MA 02138;
cheinke@cfa.harvard.edu, josh@cfa.harvard.edu, pedmonds@cfa.harvard.edu,
dlloyd@cfa.harvard.edu, ssm@cfa.harvard.edu

and

H. N. Cohn and P. M. Lugger
Department of Astronomy, Indiana University, Swain West 319, Bloomington, IN 47405;
cohn@indiana.edu, lugger@indiana.edu
Received 2003 May 22; accepted 2003 August 4

ABSTRACT

We report our analysis of a *Chandra* X-ray observation of the rich globular cluster M80, in which we detect some 19 sources to a limiting 0.5–2.5 keV X-ray luminosity of 7×10^{30} ergs s^{-1} within the half-mass radius. X-ray spectra indicate that two of these sources are quiescent low-mass X-ray binaries containing neutron stars. We identify five sources as probable cataclysmic variables (CVs), one of which seems to be heavily absorbed, implying high inclination. The brightest CV may be the X-ray counterpart of nova 1860 T Sco. The concentration of the X-ray sources within the cluster core implies an average mass of $1.2 \pm 0.2\ M_{\odot}$, consistent with the binary nature of these systems and very similar to the radial distribution of the blue stragglers in this cluster. The X-ray and blue straggler source populations in M80 are compared to those in the similar globular cluster 47 Tuc.

Subject headings: blue stragglers — globular clusters: individual (NGC 6093) — novae, cataclysmic variables — stars: neutron — X-rays: binaries

1. INTRODUCTION

The *Chandra X-Ray Observatory* has allowed rapid gains in the study of X-ray sources in globular clusters, especially when combined with the resolution of the *Hubble Space Telescope* (*HST*). Faint X-ray sources had been identified with *Einstein* (Hertz & Grindlay 1983) and *ROSAT* (see Verbunt 2001 for a review). A few of these had been identified with bright low-mass X-ray binaries (LMXBs) in quiescence (qLMXBs; e.g., Verbunt, Elson, & van Paradijs 1984) or with cataclysmic variables (Cool et al. 1995). Recently, *Chandra* (and to a lesser degree *XMM-Newton*) has allowed the identification and detailed study of scores of faint X-ray sources in 47 Tuc (Grindlay et al. 2001a, hereafter GHE01a), NGC 6397 (Grindlay et al. 2001b, hereafter GHE01b), ω Cen (Rutledge et al. 2002; Cool, Haggard, & Carlin 2002), NGC 6752 (Pooley et al. 2002b), NGC 6440 (Pooley et al. 2002a), and M28 (Becker et al. 2003), among others. Optical and radio identifications have allowed secure identifications of cataclysmic variables (CVs), chromospherically active binaries (ABs), and millisecond pulsars (MSPs); see Edmonds et al. (2003a, 2003b), Grindlay et al. (2002), and Pooley et al. (2002b) for examples. The spectral and luminosity signatures of qLMXBs, thought to emit thermal radiation from the neutron star surface (Brown, Bildsten, & Rutledge 1998), allow them to be identified easily (Rutledge et al. 2002; GHE01b). These advances make it practical to compare significant populations of X-ray sources in different globular clusters, exploring similarities or differences in properties or formation mechanisms (see Pooley et al. 2003; Heinke et al. 2003c).

In this paper, we present new *Chandra* observations of the globular cluster M80 (NGC 6093). This globular cluster has a small core radius (6''.5; Ferraro et al. 1999) and relatively high central density [$\log(\rho_0) = 4.87$, computed using the prescription of Djorgovski 1993], although it is not core-collapsed. The distance to this cluster is estimated at $10.33^{+0.8}_{-0.7}$ kpc (Brocato et al. 1998), while $E(B-V) = 0.17 \pm 0.01$ (Harris 1996, revision of 2003 February),[1] leading to a neutral hydrogen column ($N_{\rm H}$) estimate of $N_{\rm H} = 9.4(\pm 0.9) \times 10^{20}$ cm^{-2} [using $N_{\rm H}/E(B-V) = 5.5 \times 10^{21}$ cm^{-2}, from Predehl & Schmitt 1995 using $R = 3.1$]. The cluster center is given by Shara & Drissen (1995) as R.A. $16^{\rm h}17^{\rm m}02^{\rm s}.4$, decl. $-22°58'33''.8$ (J2000). Ferraro et al. (1999, 2003) have noted the unusually large number of centrally concentrated blue stragglers in M80, which are thought to have formed through collisions or dynamical hardening of close binaries. M80 is also unusual in having a known nova outburst (nova 1860 T Sco; see Shara & Drissen 1995). A *ROSAT* observation showed it to have at least one X-ray source in the core of luminosity $L_X \sim 10^{32.8}$ ergs s^{-1} (Hakala et al. 1997; Verbunt 2001).

In § 2 we describe our observations and analysis of the globular cluster M80. We discuss our findings and compare them to 47 Tuc in § 3 and provide a summary in § 4.

2. M80 OBSERVATIONS AND ANALYSIS

We observed M80 with *Chandra* for 48.6 ks on 2001 October 6 with the ACIS chip S3 at the focus (the ACIS-S aim point). This back-illuminated chip has a higher sensitivity to soft X-rays (under 4 keV, and especially below 1 keV). We reduced and analyzed the data using the *Chandra* Interactive Analysis of Observations (CIAO)[2] software. We reprocessed the level 1 event files using the latest gain files

[1] Available at http://physun.physics.mcmaster.ca/Globular.html.
[2] Available at http://asc.harvard.edu/ciao/.

and without the pixel randomization that is applied in standard data processing and filtered on grade, status, and good time intervals supplied by standard processing. We searched for, but did not find, times of elevated background. We selected an energy band of 0.5–4.5 keV to search for sources with maximum sensitivity while minimizing the background. We ran two wavelet detection algorithms, the CIAO task *wavdetect* (Freeman et al. 2002) and the *pwdetect*[3] algorithm (Damiani et al. 1997), on ACIS chip 7, with similar results. Outside the cluster half-mass radius, we select a detection sensitivity designed to identify a maximum of one spurious source on the S3 chip. In this paper we do not analyze the other four active chips.

2.1. *Detection and Colors*

In line with analyses of other clusters (e.g., Pooley et al. 2002a, 2002b, 2003), we focus our analysis on the sources within the cluster half-mass radius (39″; Harris 1996, updated 2003). This offers an excellent balance between including most cluster sources and excluding background sources. Since globular cluster X-ray sources are generally more massive than the typical cluster star, they tend to concentrate toward the center of dynamically relaxed clusters such as M80. We expect only 0.8 background active galactic nuclei (AGNs) above five counts in our 0.5–4.5 keV detection band (from Giacconi et al. 2001) within the half-mass radius.

Within the half-mass radius we choose the sensitivity of our detection algorithms to identify no more than one spurious source. However, several sources obvious to the eye remained undetected, so we further increased the sensitivity to allow calculation of as many source positions as possible and applied both algorithms in several energy bands. We compiled a list of robust (significance $>1.65\ \sigma$, more than three counts, and visually confirmed) source detections to give a final tally of 19 sources within the half-mass radius. These sources, and the extraction regions used for later analysis, are shown in Figure 1, along with the core and half-mass regions (*large circles*; astrometry is as calculated in § 2.2 below). We give these sources shorthand names (e.g., CX12), which we will use for the rest of this paper, ordered with decreasing counts in the 0.5–4.5 keV band. The cluster source names, positions, counts in three bands, and luminosities (calculated as below) are listed in Table 1. Note that excess unresolved emission remains in the core, probably representing numerous undetected sources, of which the brightest may contribute up to seven counts. At least two sources (CX9 and CX14) could be combinations of multiple sources; however, we expect the bulk of the counts in each to be due to a single source.

We used extraction regions of 1″.25 radius circles for most sources, except for fainter sources in the core and near brighter sources where confusion was an issue, where we used 1″.0 or 0″.75 extraction regions. We extract the counts of our identified sources in four bands; a soft band (0.5–1.5 keV), a hard band (1.5–6 keV), a detection (medium) band (0.5–4.5 keV), and the *ROSAT* band (0.5–2.5 keV). We define an Xcolor (following GHE01a) as $2.5 \times \log$(0.5–1.5 keV counts/1.5–6 keV counts). Our exposure map is uniform to within 1% between the locations of different cluster

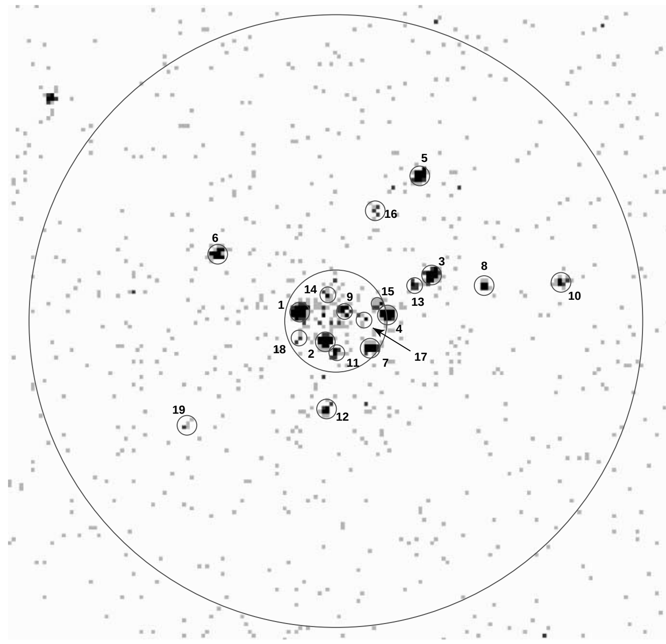

Fig. 1.—*Chandra* ACIS-S image of the globular cluster M80. The two larger circles represent the core (*inner circle*; 6″.5) and half-mass (*outer circle*; 39″) radii of the cluster. The 19 sources within the half-mass radius are labeled (in order of decreasing counts in the 0.5–4.5 keV band), and the extraction regions are overlaid. Additional X-ray emission is visible from the central cluster core from sources unresolved with *wavdetect*. CXOU J161705.1−225805 is also visible at upper left and may be associated with the cluster.

sources, so we do not make exposure corrections to the observed counts. We extracted counts from a large source-free adjacent background region to estimate the background flux, finding 0.019 counts pixel^{-1} in the 0.5–4.5 keV band, 0.011 counts pixel^{-1} in the 0.5–1.5 keV band, and 0.012 counts pixel^{-1} in the 1.5–6 keV band. Since the chance of having even one background count recorded in any band is less than 25% for our source extraction regions, we do not perform background subtraction on our extracted numbers of counts, although we do extract background spectra for spectral fitting purposes. We derive aperture corrections from the fraction of a CXC point-spread function (derived using the CIAO tool *mkpsf* for 1.6 keV, the mean energy of the core sources) that falls within our extraction circles and apply these to the luminosities below.

We also list the positions, colors, and exposure-corrected photon fluxes of sources outside the half-mass radius of the cluster, but on ACIS chip 7, in Table 2. These are derived using the wavelet detection program *pwdetect*, with the final detection significance set to $4.5\ \sigma$, leading to an expectation of less than one false source on the S3 chip. A few spurious or multiply detected sources were removed by hand, leaving 52 sources outside the cluster half-mass radius. The density of 10 count sources on the rest of the chip (0.55 arcmin^{-2}) indicates that 2.2 sources should be found between 1 and 2 cluster half-mass radii, while 3 are found. (Only 0.7 sources are expected within the half-mass radius.) Beyond 2 half-mass radii the source numbers are equal to or lower than the mean chip density of 10 count sources. The 1–2 half-mass radii overdensity is not significant at even the $1\ \sigma$ level, but we cannot rule out that one or two of these

[3] Available at
http://www.astropa.unipa.it/progetti_ricerca/PWDetect/.

TABLE 1
X-Ray Sources in M80

Source	R.A.	Decl.	Counts (0.5–4.5)	Counts (0.5–1.5)	Counts (1.5–6)	L_X (ergs s^{-1}) (0.5–6)	L_X (ergs s^{-1}) (0.5–2.5)
CX1	16 17 02.814(4)	−22 58 32.67(4)	299	172	146	$6.5 \times 10^{32}(\pm6\%)$	$3.4 \times 10^{32}(\pm6\%)$
CX2	16 17 02.576(2)	−22 58 36.48(3)	209	195	14	$2.9 \times 10^{32}(\pm7\%)$	$2.9 \times 10^{32}(\pm7\%)$
CX3	16 17 01.597(3)	−22 58 27.95(4)	148	86	68	$3.3 \times 10^{32}(\pm8\%)$	$1.9 \times 10^{32}(\pm9\%)$
CX4	16 17 02.005(4)	−22 58 33.03(5)	147	76	81	$3.8 \times 10^{32}(\pm8\%)$	$2.0 \times 10^{32}(\pm9\%)$
CX5	16 17 01.708(4)	−22 58 15.34(6)	80	37	46	$2.0 \times 10^{32}(\pm11\%)$	$9.5 \times 10^{31}(\pm13\%)$
CX6	16 17 03.569(5)	−22 58 25.30(6)	55	54	2	$9.1 \times 10^{31}(\pm13\%)$	$9.1 \times 10^{31}(\pm13\%)$
CX7	16 17 02.164(6)	−22 58 37.27(5)	50	25	25	$1.0 \times 10^{32}(\pm14\%)$	$5.7 \times 10^{31}(\pm15\%)$
CX8	16 17 01.114(5)	−22 58 29.33(8)	25	11	14	$5.1 \times 10^{31}(\pm20\%)$	$3.2 \times 10^{31}(\pm20\%)$
CX9	16 17 02.401(7)	−22 58 32.6(1)	24	14	10	$5.0 \times 10^{31}(\pm20\%)$	$2.8 \times 10^{31}(\pm22\%)$
CX10	16 17 00.407(8)	−22 58 28.87(7)	23	10	13	$4.7 \times 10^{31}(\pm21\%)$	$2.4 \times 10^{31}(\pm24\%)$
CX11	16 17 02.472(8)	−22 58 37.86(8)	21	13	9	$4.6 \times 10^{31}(\pm21\%)$	$2.2 \times 10^{31}(\pm25\%)$
CX12	16 17 02.565(7)	−22 58 45.0(1)	20	14	6	$4.1 \times 10^{31}(\pm22\%)$	$2.7 \times 10^{31}(\pm22\%)$
CX13	16 17 01.755(7)	−22 58 29.29(9)	12	5	8	$2.7 \times 10^{31}(\pm28\%)$	$1.5 \times 10^{31}(\pm30\%)$
CX14	16 17 02.553(8)	−22 58 30.5(2)	11	7	4	$2.3 \times 10^{31}(\pm30\%)$	$1.5 \times 10^{31}(\pm30\%)$
CX15	16 17 02.100(7)	−22 58 31.8(1)	9	1	13	$3.5 \times 10^{31}(\pm27\%)$*	$4 \times 10^{30}(^{+132}_{-65}\%)$*
CX16	16 17 02.119(8)	−22 58 19.8(2)	9	4	5	$1.8 \times 10^{31}(^{+46}_{-33}\%)$	$1.1 \times 10^{31}(^{+49}_{-35}\%)$
CX17	16 17 02.220(7)	−22 58 33.7(2)	8	7	1	$1.7 \times 10^{31}(^{+49}_{-35}\%)$	$1.1 \times 10^{31}(^{+49}_{-35}\%)$
CX18	16 17 02.820(7)	−22 58 36.0(2)	6	4	2	$1.3 \times 10^{31}(^{+60}_{-40}\%)$	$8 \times 10^{30}(^{+60}_{-40}\%)$
CX19	16 17 03.85(1)	−22 58 47.1(2)	5	4	1	$1.0 \times 10^{31}(^{+68}_{-43}\%)$	$7 \times 10^{30}(^{+68}_{-43}\%)$

Notes.—Units of right ascension are hours, minutes, and seconds, and units of declination are degrees, arcminutes, and arcseconds. Names, positions, counts in three X-ray energy bands (energies given in keV) and estimated luminosities of X-ray sources within the half-mass radius of M80. The errors in parentheses after the position represent the 1 σ uncertainties in the relative positions of the sources, derived from *wavdetect* results. The counts in each band are the numbers of photons within the circular source regions of Fig. 1. Luminosities have been adjusted to account for the percentage of the point spread function included in each region. The luminosities for CX1–CX6 are derived from individual spectral fittings, while the luminosities for CX7–CX19 are derived from fitting their combined (except CX15) spectrum. Luminosity errors (given in percentage) are derived from Poisson or Gehrels statistics of the detected counts in each band. *CX15 probably suffers significant intrinsic absorption, unaccounted for in these luminosities (see text).

sources are associated with the cluster. Assuming a power-law spectrum with photon index 1.7 and the cluster N_H, on the order of 22 background AGNs should be detected above 10 counts in our band over the entire chip (Giacconi et al. 2001). The 38 sources outside the cluster half-mass radius are thus a significant overdensity, implying a Galactic population of X-ray sources in line with the results of ongoing Galactic plane and bulge surveys (e.g., Grindlay et al. 2003). However, further analysis of these sources is outside the scope of this paper.

We create two versions of an "X-ray color-magnitude diagram" to assist with source classification. In the first version we follow the formalism of GHE01a, assigning the logarithm of the number of counts in the 0.5–4.5 keV band to the y-axis and X-ray color (Xcolor) to the x-axis (Fig. 2). This version explicitly uses the observational quantities. In the second version we attempt to correct the color uniformly for the cluster absorption. We use the *Chandra* proposal tool PIMMS[4] to investigate the effects of an absorbing column of 9.4×10^{20} cm^{-2} on the numbers of detected counts in our chosen bands. We use 0.2 and 0.3 keV blackbody spectra, 1, 5, and 10 keV bremsstrahlung spectra, and power-law spectra with photon index 1 or 2, which cover the range of X-ray spectral types seen in globular clusters (suggesting qLMXBs, CVs, and pulsars respectively; see references in § 1). We calculate the average difference between the calculated colors and the colors without absorption as 0.305 ± 0.025 and calculate new corrected

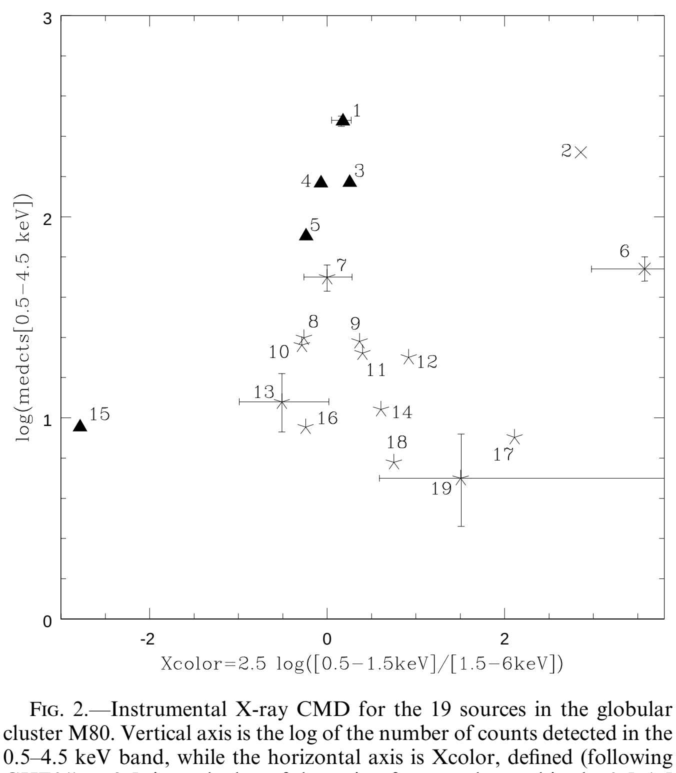

Fig. 2.—Instrumental X-ray CMD for the 19 sources in the globular cluster M80. Vertical axis is the log of the number of counts detected in the 0.5–4.5 keV band, while the horizontal axis is Xcolor, defined (following GHE01) as 2.5 times the log of the ratio of counts detected in the 0.5–1.5 keV band over the counts detected in the 1.5–6 keV band. A few error bars are shown, representing 1 σ errors of Gehrels (1986). Symbols represent probable source nature, as in GHE01; ×: qLMXBs, ▲: CVs, ⋆: ambiguous (probably a mixture of CVs and ABs). Sources are numbered as in Table 1.

[4] Available at http://asc.harvard.edu/toolkit/pimms.jsp.

TABLE 2
Serendipitous Sources in the M80 Field

Name (CXOU J)	R.A.	Decl.	Counts (0.5–4.5 keV)	Flux (photons cm^{-2} s^{-1})
161646.9−225737	16 16 46.93(2)	−22 57 37.7(3)	426.3(22.8)	1466.6(78.5)
161646.9−225509	16 16 46.98(12)	−22 55 9.9(18)	12.5(5.0)	42.6(16.9)
161647.1−225535	16 16 47.19(7)	−22 55 35.9(10)	83.2(9.2)	280.2(30.8)
161648.3−225906	16 16 48.35(7)	−22 59 6.2(10)	7.6(3.6)	25.8(12.3)
161648.5−225311	16 16 48.55(14)	−22 53 11.9(21)	24.7(7.8)	95.2(30.1)
161648.5−225752	16 16 48.55(5)	−22 57 52.4(8)	17.7(5.9)	60.4(20.2)
161648.6−225412	16 16 48.64(11)	−22 54 12.4(17)	17.0(6.1)	61.8(22.3)
161649.8−225705	16 16 49.86(2)	−22 57 5.3(3)	4.2(3.2)	14.4(11.0)
161650.2−225349	16 16 50.28(9)	−22 53 49.5(14)	10.7(4.8)	37.0(16.7)
161652.1−225612	16 16 52.15(2)	−22 56 12.9(3)	4.2(3.7)	14.0(12.4)
161652.2−225614	16 16 52.29(3)	−22 56 14.6(5)	104.3(10.7)	350.5(36.1)
161652.8−225420	16 16 52.85(12)	−22 54 20.8(18)	11.8(4.7)	42.1(16.9)
161653.8−225844	16 16 53.83(2)	−22 58 44.2(4)	23.1(7.0)	80.3(24.2)
161653.9−225618	16 16 53.93(5)	−22 56 18.8(8)	18.5(6.4)	62.3(21.5)
161653.9−225904	16 16 53.94(2)	−22 59 4.1(3)	27.2(5.1)	92.2(17.3)
161654.6−225615	16 16 54.63(6)	−22 56 15.2(10)	8.5(3.6)	28.4(12.2)
161655.0−225451	16 16 55.09(6)	−22 54 51.6(9)	118.4(11.5)	398.0(38.6)
161655.5−225925	16 16 55.58(1)	−22 59 25.7(2)	69.5(8.9)	235.5(30.1)
161655.8−225625	16 16 55.85(3)	−22 56 25.1(4)	5.0(2.8)	16.6(9.4)
161655.9−225635	16 16 55.97(3)	−22 56 35.8(4)	11.7(4.6)	41.6(16.3)
161658.3−225838	16 16 58.30(3)	−22 58 38.1(4)	5.6(3.0)	18.6(9.9)
161659.1−225349	16 16 59.14(17)	−22 53 49.5(25)	15.0(6.0)	52.9(20.9)
161659.8−225931	16 16 59.88(2)	−22 59 31.1(2)	10.0(4.3)	32.9(14.1)
161700.8−225700	16 17 0.90(5)	−22 57 0.1(7)	7.4(3.3)	29.1(13.0)
161701.0−225307	16 17 1.05(16)	−22 53 7.8(24)	16.2(6.0)	57.9(21.5)
161702.0−230033	16 17 2.05(1)	−23 0 33.0(2)	65.7(8.9)	218.0(29.6)
161704.1−225527	16 17 4.10(3)	−22 55 27.4(5)	86.7(11.2)	283.0(36.6)
161704.5−230055	16 17 4.57(4)	−23 0 55.2(6)	5.0(2.7)	16.7(9.0)
161704.7−225622	16 17 4.78(4)	−22 56 22.6(5)	5.8(2.9)	18.8(9.4)
161705.1−225805	16 17 5.10(2)	−22 58 5.5(4)	20.9(6.6)	70.1(22.1)
161706.2−225835	16 17 6.22(2)	−22 58 35.6(3)	8.7(4.2)	29.3(14.0)
161706.4−225318	16 17 6.49(16)	−22 53 18.0(24)	15.2(5.6)	53.7(19.8)
161706.8−225808	16 17 6.87(2)	−22 58 8.2(3)	29.6(5.6)	99.1(18.6)
161707.0−230121	16 17 7.06(3)	−23 1 21.3(5)	24.3(7.3)	122.7(36.8)
161707.7−225755	16 17 7.77(2)	−22 57 55.8(3)	77.6(9.3)	258.2(31.1)
161707.8−225752	16 17 7.90(3)	−22 57 52.0(4)	4.6(2.7)	15.3(8.9)
161708.2−225617	16 17 8.27(3)	−22 56 17.1(4)	4.5(2.6)	14.7(8.5)
161709.1−225529	16 17 9.20(3)	−22 55 29.1(4)	247.5(19.0)	817.7(62.7)
161709.8−230034	16 17 9.81(3)	−23 0 34.7(4)	11.1(4.4)	36.7(14.4)
161712.3−225313	16 17 12.34(8)	−22 53 13.2(11)	202.9(15.5)	1039.9(79.3)
161712.5−230034	16 17 12.51(4)	−23 0 34.4(6)	48.2(7.5)	160.6(25.1)
161713.6−225324	16 17 13.63(16)	−22 53 24.1(24)	18.1(6.6)	67.4(24.5)
161713.7−225549	16 17 13.79(6)	−22 55 49.8(9)	47.2(7.5)	156.2(25.0)
161714.6−225520	16 17 14.66(2)	−22 55 20.0(3)	13492.3(121.7)	47046.0(424.5)
161715.8−225516	16 17 15.84(5)	−22 55 16.5(7)	356.0(20.5)	1263.8(72.7)
161716.0−225857	16 17 16.04(2)	−22 58 57.4(2)	10.4(4.4)	34.9(14.7)
161716.0−225858	16 17 16.05(2)	−22 58 58.9(3)	5.1(3.3)	17.1(11.0)
161716.8−225608	16 17 16.88(5)	−22 56 8.7(8)	6.5(4.0)	21.5(13.3)
161716.9−225953	16 17 16.99(3)	−22 59 53.1(5)	116.4(11.9)	413.3(42.1)
161718.7−225512	16 17 18.71(7)	−22 55 12.0(11)	67.8(9.9)	229.8(33.4)
161719.5−225705	16 17 19.56(7)	−22 57 5.3(10)	8.7(3.9)	29.0(13.0)
161721.7−225415	16 17 21.75(15)	−22 54 15.2(23)	19.1(6.6)	66.0(22.7)

Notes.—Units of right ascension are hours, minutes, and seconds, and units of declination are degrees, arcminutes, and arcseconds. Sources outside the M80 half-mass radius detected on the S3 chip during the M80 observation. Relative positional errors are given in parentheses on the last quoted digits. Counts in the 0.5–4.5 keV band, photon flux, and errors in both are given by the *pwdetect* tool.

colors for our sources. Instead of using counts as the y-axis, we use the luminosity in the 0.5–6 keV band, where *Chandra* has its greatest sensitivity. This provides us with an X-ray CMD that can be compared directly to CMDs of other clusters (Fig. 3).

We compare Figure 3 with the results from 47 Tuc (GHE01a; Edmonds et al. 2003a, 2003b), ω Cen (Rutledge et al. 2002; Cool, Haggard, & Carlin 2002), NGC 6397 (GHE01b), NGC 6752 (Pooley et al. 2002a), NGC 6440 (Pooley et al. 2002b), and M28 (Becker et al. 2003).

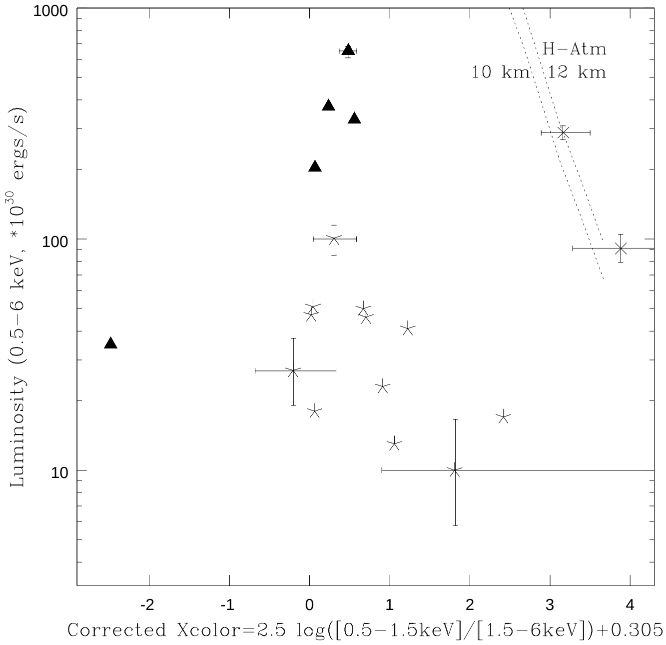

FIG. 3.—Standardized X-ray CMD for the 19 sources in the globular cluster M80. *Vertical axis*: 0.5–6 keV X-ray luminosity in units of 10^{30} ergs s^{-1}, derived from spectral fitting (see text). *Horizontal axis*: Xcolor as in Fig. 2, but with a uniform shift of 0.305 added to correct for the effects of photoelectric absorption (not including intrinsic absorption). Errors do not include spectral uncertainties. Symbols same as in Fig. 2.

Quiescent LMXBs have been identified in globular clusters by their blackbody-like spectra and high F_X/F_{opt} values. CX2 and CX6 have similar colors and luminosities to qLMXBs identified in 47 Tuc (X5, X7), ω Cen (3), NGC 6397 (U24), and NGC 6440 (CX1) by these means, so we classify them as probable qLMXBs. As a further check on our classification, we plot in Figure 3 theoretical tracks for 10 and 12 km nonmagnetic hydrogen-atmosphere models of Lloyd (2003). These are essentially cooling tracks for neutron stars, since they show how the X-ray color of the qLMXB should change as the luminosity decreases for an NS of fixed radius. Clearly, CX2 and CX6 are in agreement with the predictions of these tracks.

Harder sources ($-1 <$ Xcolor < 1) associated with these clusters above 10^{32} ergs s^{-1} seem to be almost entirely CVs (GHE01a; GHE01b; Pooley et al. 2002a), so we identify CX2, CX3, CX4, and CX5 as probable CVs. Two eclipsing CVs in 47 Tuc (W8 and W15; GHE01a; Edmonds et al. 2003a, 2003b) show Xcolor < -1 due to high intrinsic absorption of the X-rays from the inner disk and/or white dwarfs passing through the edge-on accretion disk. X-ray spectra showing these colors without high intrinsic absorption (from an accretion disk or other gas in the system) are highly implausible. CX15 shows colors and luminosities similar to these systems, so we propose it is also a CV. The remaining sources, below $L_X = 10^{32}$ ergs s^{-1}, are similar in colors and luminosity to both CV and bright AB systems in 47 Tuc, ω Cen, NGC 6397, and NGC 6752. Soft MSPs in 47 Tuc and NGC 6752 are uniformly less X-ray luminous than any systems in M80, but the unusual nonthermally emitting MSPs in NGC 6397 (GHE01b) and 47 Tuc (47 Tuc-W; Edmonds et al. 2002b) are as luminous as our faintest sources. (A luminous, young MSP such as PSR B1821-24 in M28 should probably be detected in the current radio searches of M80 by N. D'Amico et al. We believe such objects to be rare in globular clusters, but we cannot exclude such an object, as our 3.2 s readout time does not allow pulsation searches at appropriate periods.) Therefore, we regard our remaining sources as probably predominantly CVs, with some ABs and perhaps MSPs mixed in. We identify probable CVs, qLMXBs, and unidentified sources with $\blacktriangle$, $\times$, and $\star$ symbols, respectively, in Figures 2 and 3.

2.2. *Astrometry and a Possible Counterpart*

The *ROSAT* X-ray source 7, identified by Verbunt (2001) as star HD 146457 ($V = 8.46$), is clearly detected 4$'$.2 off-axis as CXOU J161714.6−225520. Five other serendipitous *ROSAT* sources also appear in the *Chandra* field of view. No other bright sources are unambiguously identified with SIMBAD objects, so we use HD 146457 to define our astrometry. We find an offset between the *Chandra wavdetect* and *pwdetect* positions and the Tycho Reference Catalog position of −0.002 s, +1$''$.66 (Tycho-*Chandra*) and add this offset to our nominal astrometric solution to derive a corrected astrometric solution, which we use for the rest of this paper. The uncertainty in the *pwdetect*-derived position of HD 146457 is $\Delta\alpha = 0^s.02$, $\Delta\delta = 0''.3$, but our absolute astrometric errors may be slightly increased because of uncertainties in the plate scale and off-axis point-spread function modeling. Analysis of numerous point sources with optical counterparts by Feigelson et al. (2002) and Muno et al. (2003) suggest that typical relative astrometric uncertainties at 4$'$ off-axis are of the order of 0$''$.5. The absolute uncertainty of *Chandra* astrometry is estimated at 0$''$.6 (90% confidence; Aldcroft et al. 2000), making this astrometric correction relatively large.

Although classification by color and luminosity can identify some X-ray sources with certain populations, optical identification of counterparts is necessary to be certain of most classifications. The full task is beyond the scope of this work, but we do consider previously identified possible counterparts. Shara & Drissen (1995) identified two faint blue stars in M80 that are candidate CVs. They identify one at R.A. $16^h17^m02^s.83$, decl. $-22°58'31''.3$ (J2000, using the Guide Star Catalog I), as the probable counterpart of nova 1860 T Sco, based on a contemporary determination (Auwers 1862) of the nova position with respect to two bright stars and the cluster center. Shara & Drissen's preferred extrapolation of the Auwers (1862) nova position (using offsets from bright stars) is R.A. $16^h17^m02^s.82$, decl. $-22°58'32''.1$. These positions are, respectively, 1$''$.4 and 0$''$.6 away from our position for CX1, the brightest candidate CV in our image. Considering the uncertainties (often 1$''$–2$''$) in the Guide Star Catalog I and in our astrometric solution above, we suggest that CX1 may be the X-ray counterpart of nova 1860 T Sco. Hakala et al. (1997) provide three arguments against the identification of nova 1860 T Sco with the (confused) *ROSAT* M80 X-ray source: the positional discrepancy, the rather high X-ray luminosity, and the rather high X-ray–to–optical flux ratio. The positional discrepancy is greatly reduced by the resolution of the *ROSAT* M80 source into numerous sources by *Chandra*. The X-ray luminosity of CX1 is only 3.1×10^{32} ergs s^{-1} (0.5–2.5 keV), compared to the total cluster L_X(0.5–2.5 keV) $\sim 8.6 \times 10^{32}$ ergs s^{-1} for the *ROSAT* PSPC observation cited by Hakala et al. (1995). While high, this luminosity is comparable to that of probable CVs in other globular clusters, e.g., 47 Tuc (GHE01a), NGC 6440 (Pooley et al. 2002a), and Terzan 5 (Heinke et al. 2003b). Finally, the (absorbed 0.5–2.5 keV) X-ray to (uncorrected V-band) optical flux ratio (F_X/F_{opt}) of CX1, if it is the counterpart of nova 1860 T Sco, is 4.5. While somewhat high for field systems, this is consistent with the range of F_X/F_{opt} found for CVs in 47 Tuc by Edmonds et al. (2003b), of which the brightest objects may be magnetic DQ Her systems (GHE01a). We note that a fainter undetected CX1 counterpart would increase the F_X/F_{opt} ratio and that, in any case, the X-ray and optical flux measurements are not simultaneous. Thus, we conclude that the association is plausible but unproven. Further *HST* analysis is in progress to look for additional X-ray counterpart candidates and improve the *Chandra*/*HST* relative astrometry.

2.3. *Spectral Fitting*

For the six brightest sources associated with the cluster (over 50 counts), we extract source (using at least 10 counts bin^{-1}) and (off-cluster) background spectra using the CIAO script *psextract* and fit the spectra in XSPEC version 11.2 (Arnaud 1996).[5] We correct the effective area functions for the time-dependent low-energy quantum efficiency degradation.[6] We exclude bins with most photons below 0.3 keV or above 10 keV. We attempt to fit three models to these spectra, all with photoelectric absorption as a free parameter forced to be equal to or greater than the cluster value (9.4×10^{20} cm^{-2}). For all analysis in this paper, we use photoelectric absorption X-ray cross sections of Balucinska-Church & McCammon (1992) in the XSPEC phabs model. Our models are a thermal bremsstrahlung spectrum as associated with CVs, a power-law model, and a hydrogen atmosphere model (Lloyd 2003), as appropriate for qLMXBs containing thermal neutron stars with $B < 10^{10}$ G, with the radius fixed at 10 km. The dichotomy between harder and softer sources apparent in the X-ray CMDs is also clear in the spectral fitting, with CX2 and CX6 showing good fits to the hydrogen atmosphere spectral models, while CX1, CX3, CX4, and CX5 do not. CX2 and CX6 require large values for a power-law photon index (>5) and very small bremsstrahlung temperatures (<0.6 keV), which are not consistent models for any known physical sources at these luminosities. CX1, CX3, CX4, and CX5 give bremsstrahlung temperatures consistent with $\sim$7 keV or more, as appropriate for luminous CVs, particularly magnetic CVs (Eracleous, Halpern, & Patterson 1991; Mukai 2001). Mekal models (Liedahl, Osterheld, & Goldstein 1995) give indistinguishable results, given the low metallicity ([Fe/H] $= -1.75$) and high temperatures. This result confirms our tentative classification of these sources as cataclysmic variables in § 2.1. We note that CX6 requires a higher N_H than the cluster value for any of our models, while the other sources are consistent with the cluster value. Heinke et al. (2003a) note enhanced N_H toward X5 and X7 in 47 Tuc, presumably from gas inside or surrounding the system. Our preferred spectral fits to these six sources are shown in Figure 4, and results for all three models are listed in Table 3.

For the remaining sources within the half-mass radius (except CX15, which has a very unusual spectrum; see § 2.1), we extract a combined spectrum and fit this to derive the mean spectral shape and luminosity/count ratio. We extract a total of 235 counts and fit them with a thermal bremsstrahlung model of $kT = 2.3^{+0.91}_{-0.64}$ keV (for fixed $N_H = 9.4 \times 10^{20}$ cm^{-2}), ($\chi^2_\nu = 1.45$ for 8 dof). A MEKAL fit gives very similar results, while fits with a power law or blackbody require very different column densities. The power law requires $N_H = 26 \pm 9 \times 10^{20}$ cm^{-2} with a photon index of $2.4^{+0.4}_{-0.3}$ ($\chi^2_\nu = 1.8$ for 8 dof), while the blackbody fit requires $N_H = 0^{+3}_{-0} \times 10^{20}$ cm^{-2}, much less than the cluster value. These results indicate that the fainter sources have lower temperatures than the bright CVs, as expected for a mix of active binaries and (perhaps nonmagnetic) CVs, as seen in 47 Tuc (Edmonds et al. 2003a, 2003b). We use the bremsstrahlung spectral fits to derive fluxes. To calculate the luminosities of each of the fainter sources, we multiplied their integrated luminosity by the ratio of each source's counts to the combined source counts (Table 1). We do this for both the 0.5–2.5 keV band and the 0.5–6 keV band. Derived luminosity errors are simply Poisson or Gehrels errors from the detected counts, without including spectral uncertainties, and are thus underestimates.

2.4. *Time Variability*

We extracted event files from each detected source within the half-mass radius and tested them using the IRAF *vartst* to attempt to disprove the hypothesis that the source flux is constant. Two sources (CX1 and CX8) showed variability at the 99% confidence level, according to both the Cramer-von Mises and Kolmogorov-Smirnov

[5] Available at http://xspec.gsfc.nasa.gov.

[6] Using the ACISABS model; see http://cxc.harvard.edu/cal/Acis/Cal_prods/qeDeg/.

TABLE 3

SPECTRAL FITS TO BRIGHTER M80 SOURCES

	H ATMOSPHERE			BREMSSTRAHLUNG			POWER LAW		
SOURCE	kT (eV)	$N_H \times 10^{20}$	χ^2_ν/dof	kT (keV)	$N_H \times 10^{20}$	χ^2_ν/dof	α	$N_H \times 10^{20}$	χ^2_ν/dof
CX1	106	39.7	3.97/29	>7.3	$9.4^{+3.3}_{-0}$	0.80/28	$1.4^{+.3}_{-.1}$	$9.4^{+5.6}_{-0}$	0.76/28
CX2	89 ± 2	$9.4^{+2.5}_{-0}$	0.56/18	$0.43^{+.11}_{-.13}$	$11.5^{+14.1}_{-2.1}$	0.55/17	$6.3^{+1.1}_{-1.4}$	54^{+19}_{-14}	0.80/17
CX3	99	52.3	3.3/13	$6.0^{+12}_{-3.0}$	$9.4^{+9.1}_{-0}$	0.43/12	$1.7^{+.5}_{-.3}$	9.4^{+15}_{-0}	0.32/12
CX4	104	72	3.88/13	$7.6^{+36}_{-3.9}$	17^{+17}_{-8}	0.50/12	$1.7^{+.5}_{-.4}$	24^{+20}_{-15}	0.53/12
CX5	108	138	4.9/7	>4.1	12^{+19}_{-3}	0.53/6	$1.4^{+.6}_{-.4}$	13^{+15}_{-4}	0.57/6
CX6	76^{+5}_{-4}	22^{+8}_{-7}	0.37/4	$0.37^{+.15}_{-.21}$	27^{+26}_{-16}	0.53/3	$6.2^{+4}_{-2.2}$	63^{+59}_{-39}	0.57/3

NOTES.—Spectral fits to cluster sources, with background subtraction, in XSPEC. Errors are 90% confidence for a single parameter; spectra are binned with 10 counts bin^{-1}. All fits include photoelectric absorption forced to be $\geq 9.4 \times 10^{20}$ cm^{-2}, the cluster N_H derived from optical studies. Hydrogen atmosphere fits are made with radius fixed to 10 km.

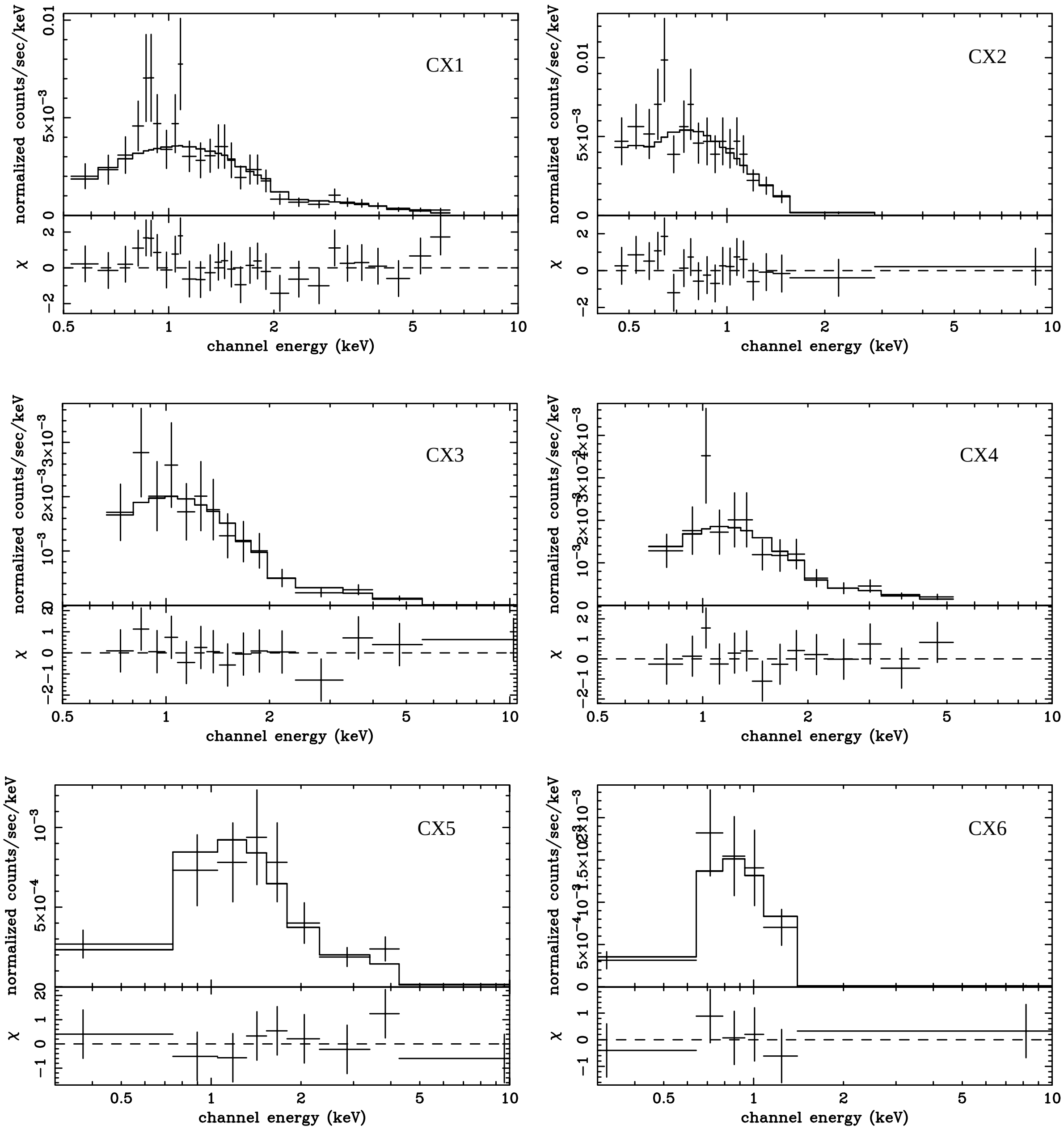

FIG. 4.—Energy spectra of six of the brighter sources in M80. *Upper panels*: Data compared with a nonmagnetic hydrogen atmosphere neutron star model (Lloyd 2003) for CX2 and CX6, and a thermal bremsstrahlung model for CX1, CX3, CX4, and CX5. *Lower panels*: Contributions to the χ^2 statistic for each fit. Photoelectric absorption is included in each fit.

tests (K-S; Daniel 1990). CX4 showed variability at the 90% confidence level in both tests, while no other source showed evidence of variability. We present the light curves from these three sources, plus the (nonvariable) light curve from CX2 (a probable qLMXB) in Figure 5. Clear flares are present in all three of the variable sources. X-ray flaring may be present in either CVs or ABs but is not expected from MSPs. The large flare visible from CX8 is reminiscent of a flare from an AB, but we cannot make any firm statements about these sources from their variability alone. The Cramer-von Mises and K-S tests are naturally far more sensitive to variability from bright sources than faint sources, so the lack of identified variability from faint sources does not indicate that they did not vary during the observation.

2.5. *Spatial Distribution of X-Ray Sources*

The radial distribution of X-ray sources in a dynamically relaxed cluster allows an estimate of the average mass of the X-ray sources. Heinke et al. (2003c) describe a procedure for estimating the typical qLMXB mass from the spatial distribution of a sample of 20 qLMXBs in seven clusters. This procedure is based on maximum-likelihood fitting of a parameterized form to the radial profile of the source distribution. The key parameter is the ratio $q = M_X/M_*$ of the source mass to the mass of the typical star that defines the optical core radius. The approach assumes that the spatial distribution of these typical stars is well described by a classic King (1966) model, which is the case for M80 (Ferraro et al. 1999). The radial profile of the source surface

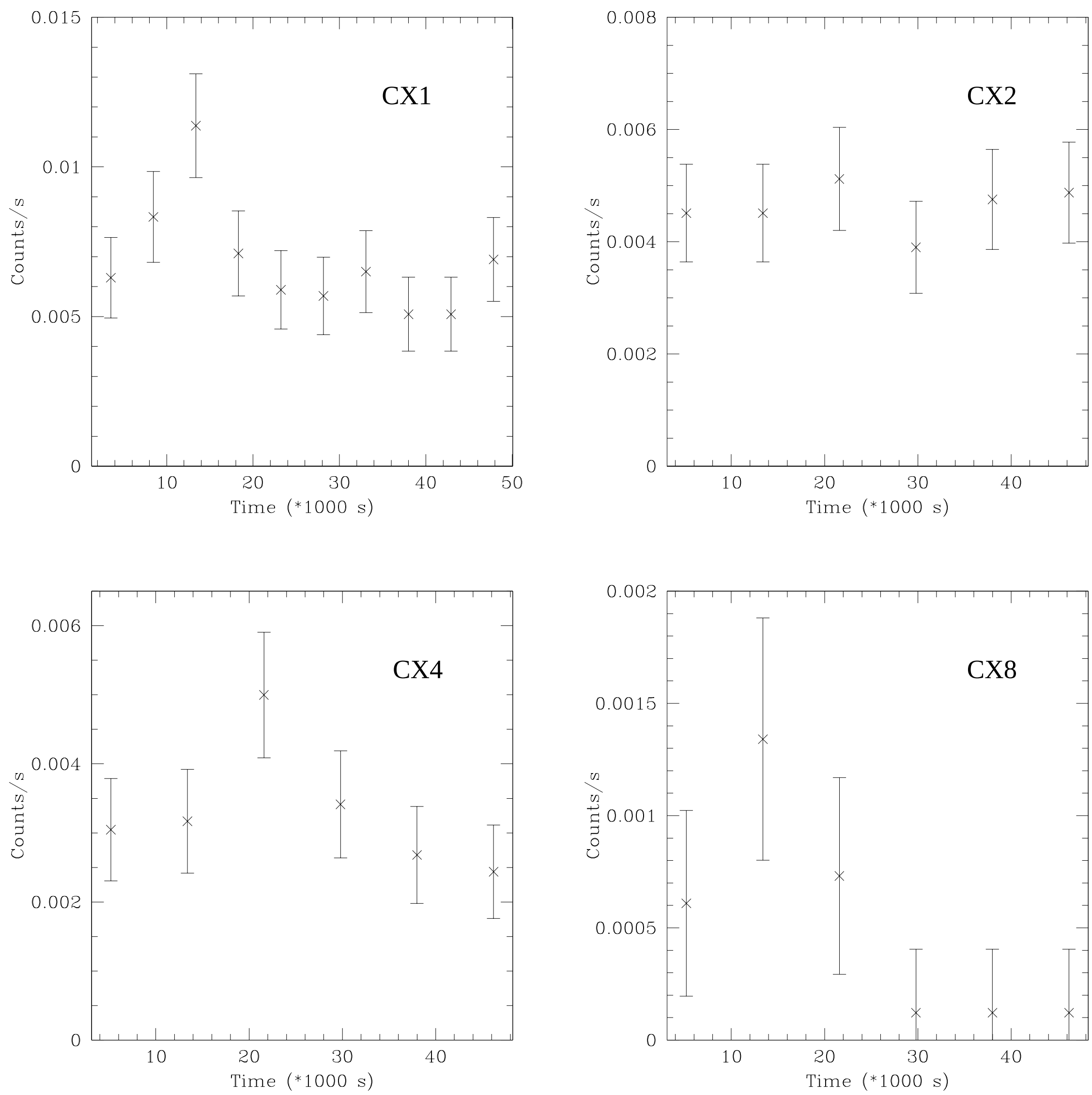

FIG. 5.—Light curves for three variable sources in M80, plus the probable qLMXB CX2 for comparison. CX1 and CX8 are found to be variable at or above the 99% level in two variability tests, while CX4 appears to be variable at the 90% level in both tests. All three of the variable sources appear to show flares.

density takes the form

$$S(r) = S_0 \left[1 + \left(\frac{r}{r_{c*}}\right)^2\right]^{(1-3q)/2} , \quad (1)$$

where S_0 is an overall normalization and r_{c*} is the optical core radius determined for turnoff-mass stars. For M80, Ferraro et al. (1999) have obtained $r_{c*} = 6''.5$.

In fitting the radial profile of the source distribution in M80, it is necessary to correct the source sample for background contamination and ensure a uniform completeness limit. We address the latter by using only sources with more than 10 counts, as we are complete to this flux limit from the cluster core out to 4 half-mass radii. The expected number of background sources above 10 counts is 0.7 sources within the half-mass radius, 2.2 between $1r_h$ and $2r_h$, 3.7 between $2r_h$ and $3r_h$, and 5.2 between $3r_h$ and $4r_h$. We correct for background using the Monte Carlo procedure described by Grindlay et al. (2002). This procedure is carried out as part of the bootstrap resampling experiment that is used to estimate the confidence ranges for the fit parameters. For each of 1000 bootstrap resamplings of the source distribution, a number of background objects is selected from a Poisson distribution with the adopted mean value for the region under consideration. A set of background object positions is then generated with a uniform random distribution over this region, and the sources that are closest to these positions are removed from the sample for that fitting trial.

Since the number of background sources beyond $2r_h$ is comparable to the total number of sources detected there, we have confined our fits to the region inside of $2r_h$. The results are nearly identical for the regions 0–$1r_h$ and 0–$2r_h$, with slightly smaller errors for the former. For this case, we obtain a mass ratio of $q = 1.44 \pm 0.22$ (1 σ) with a 90% confidence range of 1.2–2.0. For an assumed turnoff mass of approximately $M_* = 0.8\ M_\odot$, the inferred source mass is $M_X = 1.2 \pm 0.2\ M_\odot$. The 90% confidence interval extends up to 1.6 $M_\odot$. For comparison, Heinke et al. (2003c) find $q = 1.9 \pm 0.2$, corresponding to $M_X = 1.5 \pm 0.2\ M_\odot$ for the qLMXB sample. While the difference in inferred mass

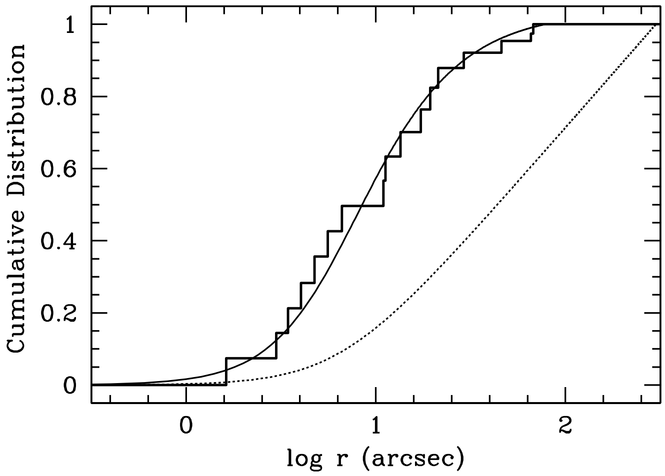

FIG. 6.—Profile fit to the background-corrected M80 source distribution. The histogram is the average of 1000 background-corrected resamplings of the original source distribution. *Smooth solid line*: Fit of eq. (1) with $q = 1.44$. *Dotted line*: Distribution of the turnoff-mass stars, i.e., eq. (1) with $q = 1$. The latter curve is normalized so that the sample is complete at 300″, the approximate outer limit of the Ferraro et al. (1999) profile.

between the M80 source sample and the pure qLMXB sample is not significant, it is in the expected direction if the former is dominated by CVs, which should have generally lower masses than qLMXBs.

Figure 6 shows the background-corrected cumulative distribution of *Chandra* sources out to $2r_h$, along with the excellent fit provided by equation (1). Also shown is the analytic King model that describes the distribution of the turnoff-mass stars. The strong central concentration of the *Chandra* sources, relative to the turnoff-mass stars, is readily apparent. The source distribution is strikingly similar to the well-determined distribution of 305 blue stragglers in M80 shown in Fig. 3 of Ferraro et al. (1999). Thus, the masses of the *Chandra* sources are likely to be quite similar to those of the blue stragglers.

2.6. *Luminosity Function and Unresolved Sources*

Pooley et al. (2002b) recently showed significant differences between the luminosity functions of several globular clusters, particularly between those of NGC 6397 and 47 Tuc. Following the method of Johnston & Verbunt (1996), they derive power-law luminosity functions $dN \propto L_X^{-\gamma} d\ln L_X$. Johnston & Verbunt (1996) found $\gamma \sim 0.58$ for 14 sources in 12 globular clusters, with rather large uncertainties, while Pooley et al. (2002b) derive γs ranging from $0.78^{+0.16}_{-0.17}$ for 47 Tuc to $0.29^{+0.11}_{-0.08}$ for NGC 6397, while NGC 6440 and NGC 6752 show intermediate values. We use the same method to constrain the luminosity function of M80, using a minimum luminosity of $L_X(0.5-2.5) = 1.5 \times 10^{31}$ ergs s^{-1}. We find a γ of $0.65^{+0.30}_{-0.20}$ as our best fit (K-S probability = 92%), with values of γ between 0.375 and 1.20 having K-S probabilities greater than 10%. Using the 0.5–6 keV luminosities instead of 0.5–2.5 keV, with a limiting luminosity of $L_X(0.5\text{–}6) = 2.0 \times 10^{31}$ ergs s^{-1}, gives a best fit γ of $0.575^{+0.23}_{-0.15}$ (K-S probability = 90%), with an acceptable range from 0.35 to 0.975. These limits are not greatly constraining, but suggest that M80's overall luminosity function is less similar to that of NGC 6397 than to the other clusters.

We address the issue of unresolved sources in the cluster core, which are clearly visible in Figure 1. We extract a total of 48 counts in the 0.5–1.5 keV band from the core outside our source regions and 37 counts in the 1.5–6 keV band. The background expected in such an area (from measurements offset from the cluster) is five soft counts and four hard counts. The expected contribution from the wings of the known cluster core sources is 23 counts in the soft band and 26 in the hard band. This leaves a total of 20 ± 9 soft counts and 7 ± 8 hard counts for the remaining core sources. (Excess emission between the core and half-mass radii cannot be determined well because of low statistics.) Visual inspection of images of the core in soft and hard bands gives the impression of additional soft sources up to perhaps six counts, while no undetected hard sources above three counts are apparent.

Although the statistics are insufficient for firm conclusions, these observations suggest that M80 has a population of fainter, softer sources than the identified sources. This is similar to the results from 47 Tuc presented by GHE01a and Grindlay et al. (2002). Such faint soft X-ray sources are likely a mixture of active binaries, MSPs, and some CVs (Edmonds et al. 2003a, 2003b). We judge our completeness limits to be roughly $L_X(0.5\text{–}2.5) = 1.5 \times 10^{31}$ and $L_X(0.5\text{–}6) = 2.0 \times 10^{31}$ ergs s^{-1} in the core, with our detection and completeness limit outside the core a factor of 2 lower. The total 0.5–2.5 keV luminosity of our unresolved M80 core emission may be of the order of 2×10^{31} ergs s^{-1}, using a 1 keV Raymond-Smith model in PIMMS. We estimate that 25% of the core is included in our known-source extraction regions. Generalized King model radial distributions for objects of twice the dominant cluster core mass (e.g., binaries and neutron stars compared to $\sim$0.7 $M_\odot$ cluster stars) tend to distribute half these objects inside one optical core radius (see Lugger, Cohn, & Grindlay 1995; Grindlay et al. 2002; Verbunt 2002). Assuming a similar distribution for undetected M80 sources suggests a total luminosity of fainter sources 2.7 times that detected, e.g., $L_X(0.5\text{–}2.5) \sim 5 \times 10^{31}$ ergs s^{-1}. The population of detected sources in 47 Tuc from 10^{30}–10^{31} ergs s^{-1} is some 68 sources totaling 2.1×10^{32} ergs s^{-1} (GHE01a), with an additional fainter unresolved emission of $\sim 7 \times 10^{31}$ ergs s^{-1} (Grindlay et al. 2002). The total luminosity of detected and undetected sources in M80 below 10^{31} ergs s^{-1} (0.5–2.5 keV) may be 7×10^{31} ergs s^{-1}. Therefore, we find that M80 probably has a population of fainter X-ray sources perhaps 25% as numerous as those in 47 Tuc.

3. DISCUSSION

The rates of close encounters between stars in globular clusters are thought to scale with the square of the central density, the volume of the core, and inversely with the velocity dispersion, $\Gamma \propto \rho_0^2 r_c^3/\sigma$, or for a King model $\Gamma \propto \rho_0^{1.5} r_c^2$ (Verbunt & Hut 1987; Verbunt 2003). According to this calculation, the production of close encounter products in 47 Tuc should be 2.0 times larger than in M80. This calculation does not account for the detailed dynamical history of the cluster, including factors such as mass segregation, core collapse, and possible destruction of wide binaries in dense environments. However, the similar central densities ($\rho_0 = 4.76$ and 4.87), central concentration parameters ($c \sim 2.0$), and total inferred masses ($M \sim 10^{6.1}$ and $10^6\ M_\odot$; Pryor & Meylan 1993) for 47 Tuc and M80, respectively, make them a reasonable comparison. We identify three differences between the two: a larger core in 47 Tuc than M80, a substantial metallicity difference between 47 Tuc and M80 ([Fe/H] is −0.76 and −1.75 of solar, respectively; Harris 1996), and a possibly high tidal destruction rate for M80 in the Galactic potential (Dinescu, Girard, & van Altena 1999; M80's orbit is somewhat chaotic, which makes this prediction uncertain).

The brighter X-ray population of M80 seems to be quite similar to that of 47 Tuc (GHE01a): each has two qLMXBs and three CVs brighter than 10^{32} ergs s^{-1}. This makes M80 somewhat richer than expected, given its smaller core. Differences may appear in the fainter X-ray sources, where M80 has 16 sources harder than qLMXBs above 10^{31} ergs s^{-1} while 47 Tuc has 24 (inside its half-mass radius; C. O. Heinke et al. 2003, in preparation; GHE01a's smaller area of study identified 18). 47 Tuc may have perhaps four times as much X-ray emission from sources below 10^{31} ergs s^{-1} and may have a steeper luminosity function (see §§ 2.5 and 2.6 above). The fainter sources in 47 Tuc are a mixture of ABs, faint CVs, and MSPs (probably 30–40 above $L_X = 10^{30}$ ergs s^{-1}; Edmonds et al. 2003b). Given the existence of two accreting neutron stars in M80, it seems unlikely that M80 is much poorer in MSPs than 47 Tuc, but radio timing surveys now underway may soon constrain the M80 MSP population. Possible subtle differences between the clusters, if confirmed, may be caused by differences in metallicity or dynamical history, including destruction effects. A larger group of globular clusters is compared in Heinke et al. (2003c) and in Pooley et al. (2003) to investigate these and other differences and their effects on X-ray source production.

M80 is unusual in having over 300 identified blue straggler stars in its central regions (Ferraro et al. 1999). Ferraro and collaborators claim that stellar density alone cannot explain this large number (citing the much smaller number in 47 Tuc) and suggest that the large blue straggler population in M80 may be due to its dynamical state on the edge of core collapse. At this stage globular clusters are expected to destroy their binary populations to avert core collapse, possibly producing large quantities of blue stragglers (Fregeau et al. 2003). However, we note that a similarly thorough search for blue stragglers over the central several core radii of 47 Tuc has not yet been done. Ferraro et al.'s (1999) observations of M80 included roughly three core radii on the PC chip, and their searches also extended to the WF chips. Ferraro et al. (2001) identified 43 blue stragglers in just one pointing of *HST* PC images of 47 Tuc (which did not fully cover the core). This included 36 greater than 0.8 mag in $m_{\rm F218W}$ above the turnoff, comparable in brightness to the 129 bright blue stragglers identified in M80 by Ferraro et al. (1999). Assuming a radial distribution of blue stragglers in 47 Tuc similar to that in M80 (Ferraro et al. 1999), we may expect some 130 bright blue stragglers in 47 Tuc, similar to the M80 population. Considering the similarity in the X-ray source populations, this suggests that many blue stragglers are produced by the same mechanisms that produce X-ray binaries. Ferraro et al. (2003) indeed find a good correlation between central density and blue straggler specific frequency for most globular clusters they study, although another formation route (probably primordial binaries) seems to be required to explain the blue stragglers in low-density environments such as NGC 288 and the outer regions of M3. It will be of interest to see if these other routes also produce X-ray sources.

4. CONCLUSION

The globular cluster M80 has a varied X-ray population similar to that of 47 Tuc (GHE01a), including two soft sources that are probable qLMXBs, numerous hard sources that are probable CVs (including one probable high-inclination system with high extinction), and a sizable population of fainter X-ray sources. The two bright soft sources fall upon a calculated neutron star cooling track in an X-ray CMD and are spectrally fitted with hydrogen-atmosphere neutron star models. The brightest CV in the cluster may be the X-ray counterpart of the old nova 1860 T Sco. The radial distribution of the X-ray sources above 10 counts indicates an average system mass of 1.2 ± 0.2 $M_\odot$ and is similar to the distribution of blue stragglers in the cluster. This is consistent with a mix of binaries containing neutron stars and lighter binaries. The overall X-ray population is slightly larger than expected when the cluster parameters are compared to those of 47 Tuc: this may be connected to the cluster's unusual orbit. The blue straggler population in M80 may be similar to that in 47 Tuc, and we hope that further theoretical and observational studies will probe the connections between these different tracers of binary hardening and exchange.

C. O. H. acknowledges support from *Chandra* grant GO2-3059A.

REFERENCES

Aldcroft, T. L., Karovska, M., Cresitello-Ditmar, M. L., Cameron, R. A., & Markevitch, M. L. 2000, Proc. SPIE, 4012, 650

Arnaud, K. A. 1996, in ASP Conf. Ser. 101, Astronomical Data Analysis Software and Systems V, ed. G. Jacoby & J. Barnes (San Francisco: ASP), 17

Auwers, G. F. 1862, Astron. Nachr., 58, 374

Balucinska-Church, M., & McCammon, D. 1992, ApJ, 400, 699

Becker, W., et al. 2003, ApJ, 585, 494

Brocato, E., Castellani, V., Scotti, G. A., Saviane, I., Piotto, G., & Ferraro, F. R. 1998, A&A, 335, 929

Brown, E. F., Bildsten, L., & Rutledge, R. E. 1998, ApJ, 504, L95 (BBR)

Cool, A. M., Grindlay, J. E., Cohn, H. N., Lugger, P. M., & Slavin, S. D. 1995, ApJ, 439, 695

Cool, A. M., Haggard, D., & Carlin, J. L. 2002, in ASP Conf. Ser. 265, Omega Centauri: A Unique Window into Astrophysics, ed. F. van Leeuwen, J. D. Hughes, & G. Piotto (San Francisco: ASP), 277

Damiani, F., Maggio, A., Micela, G., & Sciortino, S. 1997, ApJ, 483, 370

Daniel, W. W. 1990, Applied Nonparametric Statistics (2d ed.; PWS: Kent)

Dinescu, D. I., Girard, T. M., & van Altena, W. F. 1999, AJ, 117, 1792

Djorgovski, S. 1993, in ASP Conf. Ser. 50, Structure and Dynamics of Globular Clusters, ed. S. G. Djorgovski & G. Maylan (San Francisco: ASP), 373

Edmonds, P. D., Gilliland, R. E., Heinke, C. O., & Grindlay, J. E. 2003a, ApJ, 596, 1177

———. 2003b, ApJ, 596, 1197

Eracleous, M., Halpern, J., & Patterson, J. 1991, ApJ, 382, 290

Feigelson, E. D., Broos, P., Gaffney, J. A., Garmire, G., Hillenbrand, L. A., Pravdo, S. H., Townsley, L., & Tsuboi, Y. 2002, ApJ, 574, 258

Ferraro, F. R., D'Amico, N., Possenti, A., Mignani, R. P., & Paltrinieri, B. 2001, ApJ, 561, 337

Ferraro, F. R., Paltrinieri, B., Rood, R. T., & Dorman, B. 1999, ApJ, 522, 983

Ferraro, F. R., Sills, A., Rood, R. T., Paltrinieri, B., & Buonanno, R. 2003, ApJ, 588, 464

Freeman, P. E., Kashyap, V., Rosner, R., & Lamb, D. Q. 2002, ApJS, 138, 185

Fregeau, J. M., Gürkan, M. A., Joshi, K. J., & Rasio, F. A. 2003, ApJ, 593, 772

Gehrels, N. 1986, ApJ, 303, 336

Giacconi, R., et al. 2001, ApJ, 551, 624
Grindlay, J. E., Camilo, F., Heinke, C. O., Edmonds, P. D., Cohn, H., & Lugger, P. 2002, ApJ, 581, 470
Grindlay, J. E., Heinke, C. O., Edmonds, P. D., & Murray, S. S. 2001a, Science, 292, 2290 (GHE01a)
Grindlay, J. E., Heinke, C. O., Edmonds, P. D., Murray, S. S., & Cool, A. M. 2001b, ApJ, 563, L53 (GHE01b)
Grindlay, J., et al. 2003, Astron. Nachr., 324, 57
Hakala, P. J., Charles, P. A., Johnston, H. M., & Verbunt, F. 1997, MNRAS, 285, 693
Harris, W. E. 1996, AJ, 112, 1487
Heinke, C. O., Edmonds, P. D., Grindlay, J. E., Lloyd, D. A., Cohn, H. N., & Lugger, P. M. 2003b, ApJ, 590, 809
Heinke, C. O., Grindlay, J. E., Lloyd, D. A., & Edmonds, P. D. 2003a, ApJ, 588, 452
Heinke, C. O., Grindlay, J. E., Lugger, P. M., Cohn, H. N., Edmonds, P. D., Lloyd, D. A., & Cool, A. M. 2003c, ApJ, 598, 501
Hertz, P., & Grindlay, J. E. 1983, ApJ, 275, 105
Johnston, H. M., & Verbunt, F. 1996, A&A, 312, 80
King, I. R. 1966, AJ, 71, 64
Liedahl, D. A., Osterheld, A. L., & Goldstein, W. H. 1995, ApJ, 438, L115
Lloyd, D. A. 2003, MNRAS, in press
Lugger, P. M., Cohn, H. N., & Grindlay, J. E. 1995, ApJ, 439, 191
Mukai, K. 2001, preprint (astro-ph/0112048)
Muno, M. P., et al. 2003, ApJ, 589, 225
Pooley, D., et al. 2002a, ApJ, 569, 405
———. 2002b, ApJ, 573, 184
———. 2003, ApJ, 591, L131
Predehl, P., & Schmitt, J. H. M. M. 1995, A&A, 293, 889
Pryor, C., & Meylan, G. 1993, in ASP Conf. Ser. 50, Structure and Dynamics of Globular Clusters, ed. S. G. Djorgovski & G. Maylan (San Francisco: ASP), 357
Rutledge, R. E., Bildsten, L., Brown, E. F., Pavlov, G. G., & Zavlin, V. E. 2002, ApJ, 578, 405
Shara, M. M., & Drissen, L. 1995, ApJ, 448, 203
Verbunt, F. 2001, A&A, 368, 137
———. 2002, in ASP Conf. Ser. 265, ω Centauri: A Unique Window in Astrophysics, ed. F. van Leeuwen, J. Piotto, & G. Hughes (San Francisco: ASP), 289
———. 2003, in ASP Conf. Ser. 296, New Horizons in Globular Cluster Astronomy, ed. J. Piotto, G. Meylan, S. Djorgovski, & M. Riello (San Francisco: ASP), in press
Verbunt, F., Elson, R., & van Paradijs, J. 1984, MNRAS, 210, 899
Verbunt, F. & Hut, P. 1987, in IAU Symp. 125, Origin and Evolution of Neutron Stars, ed. D. J. Helfand & J.-H. Huang (Dordrecht: Reidel), 187